Percolation thresholds for rod-like particles: polydispersity effects

2008 J. Phys.: Condens. Matter 20 255250

(http://iopscience.iop.org/0953-8984/20/25/255250)

J. Phys.: Condens. Matter **20** (2008) 255250 (5pp) doi:10.1088/0953-8984/20/25/255250

Percolation thresholds for rod-like particles: polydispersity effects

Avik P Chatterjee

Department of Chemistry, 121 Edwin C Jahn Laboratory, SUNY-ESF, One Forestry Drive, Syracuse, NY 13210, USA

E-mail: apchatte@esf.edu

Received 24 January 2008, in final form 30 April 2008
Published 28 May 2008
Online at stacks.iop.org/JPhysCM/20/255250

Abstract
A model based upon excluded volume considerations is presented for the connectedness percolation thresholds in polydisperse systems of cylindrical rod-like nanoparticles. The dependence of the percolation threshold upon polydispersity index and number-averaged aspect ratio is examined for two different distribution functions for the rod radii and lengths. The importance of accounting for polydispersity is explored in the context of measurements of the elastic moduli and electrical conductance in fibre-filled nanocomposites.

1. Introduction

It has been frequently suggested that the formation of geometrically connected, percolating networks of rod-like filler particles plays a key role in the mechanical reinforcement and conductive properties, both electrical and thermal, of composite materials [1–6]. The critical particulate volume fraction at which a percolating cluster is initially formed depends strongly on the aspect ratio of the filler species [7], and is referred to as the percolation threshold [8]. The dependence of the percolation threshold upon aspect ratio has been investigated extensively in studies employing excluded volume arguments [9–12] and computer simulation techniques [7, 11, 13], as well as integral equation methods [14]. Although percolation in a population of polydisperse spheres has been examined recently [15], such theoretical efforts have focused primarily upon monodisperse systems of rod-like particles which are characterized by a sharp, well-defined aspect ratio. The assumption that filler particles are describable by a single, average aspect ratio, i.e. that they are effectively monodisperse with regards to shape, underlies several efforts to model the elastic coefficients of fibre-reinforced nanocomposites [1, 16–18]. However, recent experiments reveal that nanoparticles derived from natural sources, e.g. whiskers of nanocrystalline cellulose, typically exhibit significant degrees of polydispersity with respect to both particle lengths and widths [19–21]. Polydispersity with respect to the diameter has been reported for individual single-walled carbon nanotubes (SWNTs) grown by chemical vapour deposition [22], and may also appear as a consequence of imperfect dispersion, lateral bundling, and agglomeration within SWNT-filled composites [23, 24].

The present report generalizes a mean-field, excluded volume-based model for the percolation threshold [9, 10] to treat polydisperse systems of cylindrical rods. The percolation thresholds for subgroups of the rod population are expressed in terms of the particle dimensions by determining the mean number of inter-particle contacts as a function of the volume fraction, aspect ratio, and size distribution. Illustrative calculations are performed for two choices of the particle size distribution function. Preliminary applications of our model are presented for cellulose whisker and fibre-based composites. The approach developed in this account provides a step towards addressing effects due to particle size (and shape) polydispersity in fibre-filled nanomaterials.

2. Random contact model for the percolation threshold in polydisperse systems

We consider a polydisperse system of isotropically oriented, rigid, cylindrical rod-like particles, for which the symbol ρ denotes the number of rods (of all radii R and lengths L) per unit volume. Through suitable choices for the radii and aspect ratios, this model may be used to describe composites reinforced by carbon nanotubes [4], silicate nanorods [25], or whiskers of nanocrystalline cellulose [1, 2]. The rods are assumed to be located with respect to each other in a spatially uncorrelated, random, and homogeneous manner. A distribution function $f(R, L)$ is defined such that $f(R, L)\,\mathrm{d}R\,\mathrm{d}L$ is the number fraction of rods with radii

and lengths within the intervals $(R, R + \mathrm{d}R)$ and $(L, L + \mathrm{d}L)$, respectively. The function $f(R, L)$ is normalized by requiring that $\int_0^\infty \mathrm{d}R \int_0^\infty \mathrm{d}L\, f(R, L) = 1$. The overall rod volume fraction, denoted ϕ, is thus given by: $\phi = \pi\rho \int_0^\infty \mathrm{d}R \int_0^\infty \mathrm{d}L R^2 L f(R, L)$. Within the framework of the random contact model, the average number of contacts (designated n_c) which an individual rod of radius R_1 and length L_1 experiences with all the other rods in the system is [9, 10]:

$$n_c(R_1, L_1, \phi) = \left(\frac{\rho}{2}\right) \int_0^\infty \mathrm{d}R_2 \int_0^\infty \mathrm{d}L_2\, f(R_2, L_2) V_{12}^e (R_1, R_2, L_1, L_2), \quad (1)$$

where V_{12}^e represents the excluded volume between a pair of rods with radii and lengths (R_1, R_2) and (L_1, L_2), respectively. For an isotropic rod orientational distribution function, the angle-averaged excluded volume V_{12}^e is [26]:

$$V_{12}^e = \pi(R_1^2 L_1 + R_2^2 L_2) + \left(\frac{\pi}{2}\right)[(\pi R_1 R_2 + L_1 L_2) \times (R_1 + R_2) + \pi R_1 R_2 (L_1 + L_2) + R_1^2 L_2 + R_2^2 L_1]. \quad (2)$$

We assume that for a randomly chosen rod of radius R_1 and length L_1 to have a non-zero probability of belonging to a percolating network, such a rod must on average experience a critical minimum number of contacts [7, 9] (denoted n_c^*) with the other rods in the system, where n_c^* is treated as being independent of R_1 and L_1. It should be pointed out that Monte Carlo simulation-based investigations [7, 11, 13] of monodisperse rod systems find a weak dependence of n_c^* upon R_1 and L_1, particularly for modest aspect ratios (for example [11], reports a reduction by approximately 20% in n_c^* when the rod aspect ratio is increased by an order of magnitude). Our present work neglects this dependence, which is an approximation whose accuracy is expected to improve with increasing aspect ratios [7, 11]. Within these approximations, the critical rod volume fraction above which the percolation probability (i.e. the probability of belonging to a percolating cluster) becomes non-zero for rods with radius R_1 and length L_1 is:

$$\phi^*(R_1, L_1) = \frac{2\pi n_c^* \int_0^\infty \mathrm{d}R \int_0^\infty \mathrm{d}L\, R^2 L f(R, L)}{\int_0^\infty \mathrm{d}R_2 \int_0^\infty \mathrm{d}L_2\, f(R_2, L_2) V_{12}^e(R_1, R_2, L_1, L_2)} = \{2n_c^* \langle R^2 L\rangle\}\{[R_1^2 L_1 + \langle R^2 L\rangle + (\tfrac{1}{2})\{R_1(R_1 + L_1)(\pi\langle R\rangle + \langle L\rangle) + (\pi R_1 + L_1)(\langle RL\rangle + \langle R^2\rangle)\}]\}^{-1}, \quad (3)$$

where the averages $\langle R^p L^q\rangle$ are defined as: $\langle R^p L^q\rangle = \int_0^\infty \mathrm{d}R \int_0^\infty \mathrm{d}L f(R, L) R^p L^q$. The result presented in equation (3) is derived from equations (1) and (2) by imposing the requirement that $n_c(R_1, L_1, \phi^*) = n_c^*$ at the percolation threshold. The value of the rod volume fraction $\phi^*(R_1, L_1)$ for which the condition that $n_c(R_1, L_1, \phi) = n_c^*$ is satisfied clearly varies with the dimensions (R_1, L_1) of the particular particle in question. The 'percolation threshold' for a polydisperse system is therefore broadened into a range of volume fractions over which particles of varying sizes and aspect ratios acquire non-zero percolation probabilities in a continuous manner. Equation (3) provides a model for this dependence of the overall rod volume fraction at the percolation threshold upon R_1, L_1, and $f(R, L)$. For a specified distribution function $f(R, L)$, we denote by $\phi_{\min}^*$ the smallest rod volume fraction for which at least some of the rods in the sample population exhibit a non-vanishing percolation probability. Conversely, we let $\phi_{\max}^*$ denote the rod volume fraction above which the condition: $n_c(R_1, L_1, \phi) \geqslant n_c^*$ is satisfied for all the rods in the system. We calculate $\phi_{\min}^*(\phi_{\max}^*)$ by minimizing (maximizing) the right-hand-side of equation (3) with respect to R_1 and L_1 over the ranges of these variables for which $f(R_1, L_1)$ is non-zero. For the special case of a perfectly monodisperse system in which all the rods have identical radii R_0 and lengths L_0, the distribution function $f(R, L)$ is: $f(R, L) = \delta(L - L_0)\delta(R - R_0)$, where '$\delta$' represents the Dirac delta function. For such a monodisperse system, $\phi_{\min}^*$ and $\phi_{\max}^*$ are equal and can be expressed as:

$$\phi_{\min}^* = \phi_{\max}^* = \phi_{\text{monodisperse}}^* = \frac{2n_c^*\,(L_0/R_0)}{\left[(L_0/R_0)^2 + (\pi + 3)\,(L_0/R_0) + \pi\right]}. \quad (4)$$

In investigating the consequences of equation (3), we consider the following pair of models (designated Types I and II) for the distribution function $f(R, L)$:

Type I: In this case, we assume that all rods in the system have identical radii, denoted R_0, and vary only with respect to their lengths and aspect ratios. We define the rod aspect ratio, denoted ψ, as the ratio between the length and radius of a given rod, i.e. $\psi = L/R$. The distribution function $f(R, L)$ in this instance becomes: $f(R, L) = f_L(L)\delta(R - R_0)$, and equations (2) and (3) lead to:

$$\phi^*(R_0, L_1) = \frac{2n_c^*\,(L_n/R_0)}{\left\{\left(\frac{L_1}{R_0}\right)\left[\left(\frac{L_n}{R_0}\right) + \frac{(3+\pi)}{2}\right] + \pi + \left(\frac{3+\pi}{2}\right)\left(\frac{L_n}{R_0}\right)\right\}}, \quad (5)$$

where L_n denotes the number-averaged rod length, defined as: $L_n = \langle L\rangle = \int_0^\infty \mathrm{d}R \int_0^\infty \mathrm{d}L\, f(R, L) L$. For fixed values of L_n and n_c^*, the threshold $\phi^*(R_0, L_1)$ is minimal (maximal) for the longest (shortest) rods in the system, whose lengths we denote $L_{\max}(L_{\min})$. Furthermore, for any acceptable specification of the rod length distribution function f_L which has an upper cutoff such that f_L vanishes when L exceeds $L_{\max}$, it can be shown that for a fixed value of $(L_{\max}/R_0)$, the percolation threshold $\phi_{\min}^*$ is always lower for a polydisperse than for a monodisperse sample (for which $f_L(L) = \delta(L - L_{\max})$). Similarly, for any acceptable rod length distribution function f_L which has a lower cutoff such that f_L vanishes when L is smaller than $L_{\min}$, it can be shown that for a fixed value of $(L_{\min}/R_0)$, the percolation threshold $\phi_{\max}^*$ is always larger for a polydisperse than for a monodisperse sample (for which $f_L(L) = \delta(L - L_{\min})$). Given that n_c^* is expected to increase somewhat with decreasing aspect ratios [7, 11, 13], estimates for $\phi_{\max}^*$ based upon this model for polydispersity are likely to underestimate the exact values as determined from (say) Monte Carlo simulations.

Type II: In this case, we assume that all rods in the system have identical aspect ratios ψ, while their radii and lengths vary in a perfectly correlated manner, i.e., that $f(R, L)$ is given by: $f(R, L) = f_R(R)\delta(L - \psi R)$. This model is motivated by a recent study of nanocrystalline cellulose whiskers derived from a range of source materials [20], which

found strongly correlated variations in the lengths and widths of these nanoparticles. Equations (2) and (3) now yield:

$$\phi^*(R_1, L_1 = \psi R_1) = \frac{4n_c^*\psi\langle R^3\rangle}{\{2\psi(R_1^3 + \langle R^3\rangle) + (1+\psi)(\pi+\psi)(R_1^2\langle R\rangle + R_1\langle R^2\rangle)\}}, \tag{6}$$

where the nth moment of the rod radius distribution, denoted $\langle R^n\rangle$ is defined as: $\langle R^n\rangle = \int_0^\infty \mathrm{d}R \int_0^\infty \mathrm{d}L\, f(R, L)R^n$. For a specified distribution function $f(R, L)$ of this type, the percolation threshold $\phi^*(R_1, L_1 = \psi R_1)$ is minimal (maximal) for the largest (smallest) rods in the population, whose radii and lengths we denote respectively $R_{\max}(R_{\min})$ and $L_{\max}(L_{\min}) = \psi R_{\max}(\psi R_{\min})$. Additionally, for any acceptable specification of the distribution function f_R which has an upper cutoff such that f_R vanishes when R exceeds $R_{\max}$, it can be shown that for fixed values of $R_{\max}$ and ψ, the percolation threshold $\phi^*_{\min}$ is always lower for a polydisperse than for a monodisperse sample (for which $f_R = \delta(R - R_{\max})$). Similarly, for any acceptable specification of the distribution function f_R which has a lower cutoff such that f_R vanishes when R is smaller than $R_{\min}$, it can be shown that for fixed values of $R_{\min}$ and ψ, the percolation threshold $\phi^*_{\max}$ is always larger for a polydisperse than for a monodisperse sample (for which $f_R = \delta(R - R_{\min})$). It is to be noted that equation (6) involves the first three moments of the rod size distribution, whereas only the first moment of the rod length appears in equation (5).

3. Results and concluding remarks

We next perform illustrative calculations to explore the consequences of equations (5) and (6) for the uniform distribution function specified below:

$$\begin{aligned} f_x(x) &= 0, & x &< x_{\min}, \\ f_x(x) &= 1/(x_{\max} - x_{\min}), & x_{\min} &\leqslant x \leqslant x_{\max}, \quad \text{and} \\ f_x(x) &= 0, & x_{\max} &< x, \end{aligned} \tag{7}$$

where the variable x corresponds respectively to L and R for the aforementioned Type I and Type II polydispersity models. In each case, the rod shape distribution is prescribed by specifying (i) the number-averaged aspect ratio ψ_n, defined as: $\psi_n = \int_0^\infty \mathrm{d}R \int_0^\infty \mathrm{d}L\, f(R, L)(L/R)$, and (ii) the ratio of the length-averaged rod length L_l, defined as: $L_l = \int_0^\infty \mathrm{d}R \int_0^\infty \mathrm{d}L L^2 f(R, L)/L_n$, to the number-averaged rod length L_n. We employ the symbol P_L to denote the ratio of the length-averaged to the number-averaged rod lengths, i.e. $P_L = L_l/L_n$. Following the approach adopted in [20], we treat this quantity as a polydispersity index for the system of rods. For the uniform distribution adopted in equation (7), P_L is restricted to the range $(1 \leqslant P_L \leqslant 4/3)$, as otherwise $x_{\min}$ must adopt unphysical negative values. This range of P_L includes the polydispersities of all the samples examined in [20] with the exception of the whiskers derived from tunicin, although the nature of the function $f(R, L)$ reported in that study [20] differs significantly from the simplified model adopted in equation (7). The parameters $(L_{\min}, L_{\max})$ and $(R_{\min}, R_{\max})$, as well as the required moments of the rod length/radius distributions, are determined in terms of ψ_n and P_L. The percolation thresholds $\phi^*_{\min}(\phi^*_{\max})$ are then obtained by substituting $L_{\max}(L_{\min})$ for L_1 and $R_{\max}$ $(R_{\min})$ for R_1 in equations (5) and (6), respectively.

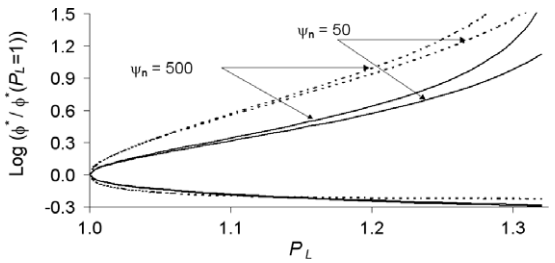

Figure 1. The rod volume fractions at the percolation thresholds $\phi^*_{\min}$ and $\phi^*_{\max}$, normalized by their values for a monodisperse system, are shown as functions of the polydispersity index P_L for fixed values of the number-averaged aspect ratio ψ_n. In each case, the upper (lower) branches of the curves represent $\phi^*_{\max}(\phi^*_{\min})$ as functions of P_L. The solid and broken lines correspond to results from Type I and Type II models for the rod shape distribution functions, respectively. For each pair of curves (solid and broken), ψ_n equals 50 and 500, in that order of increasing deviation from the line $\phi^*/\phi^*(P_L = 1) = 1$. The lower pairs of solid and broken curves appear nearly coincident and indistinguishable on the scale of the figure.

For the model calculations presented below, the critical number of inter-particle contacts per rod at the onset of percolation (n_c^*) is chosen to equal 0.6 independent of R and L. Our selection of this specific value for n_c^* enforces quantitative agreement with the asymptotic dependence reported for monodisperse systems with large aspect ratios in the computer simulation study of [7]. Additionally, if we consider hexagonal SWNT bundles with effective radii of 2.1 nm and lengths of 3 μm (wherein each bundle comprises seven individual nanotubes [23]), equation (4) together with the choice $n_c^* = 0.6$ suggests a percolation threshold located at $\phi^*_{\text{monodisperse}} \approx 8.4 \times 10^{-4}$ (or 0.084% by volume). This estimate, which assumes that (i) the bundles themselves are of uniform dimensions, and that (ii) every individual nanotube is a member of such a bundle, is consistent with the observation of a sharp increase in electrical conductivity by approximately nine orders of magnitude [23] when the SWNT volume fraction is increased from 0.02% to 0.1%.

Figure 1 displays the dependences of $\phi^*_{\min}$ and $\phi^*_{\max}$ upon the polydispersity index P_L for fixed values of the number-averaged aspect ratio ψ_n. The dependences of $\phi^*_{\min}$ and $\phi^*_{\max}$ upon ψ_n for fixed values of P_L are presented in figure 2. A broken line in figure 2 indicates the inverse dependence $(\phi^* \propto 1/\psi_n)$ expected asymptotically in the limit of large aspect ratios [7, 9, 10]. Results for a monodisperse system, calculated within the present model from equation (4), correspond to the filled diamonds in figure 2. The open squares in figure 2 represent the threshold for a monodisperse system evaluated from equation (8) of [7], which accurately describes the findings of the computer simulations reported in that study for aspect ratios $\psi \geqslant 20$ (see figure 4 of [7]). In each case, polydispersity in the rod population lowers (elevates)

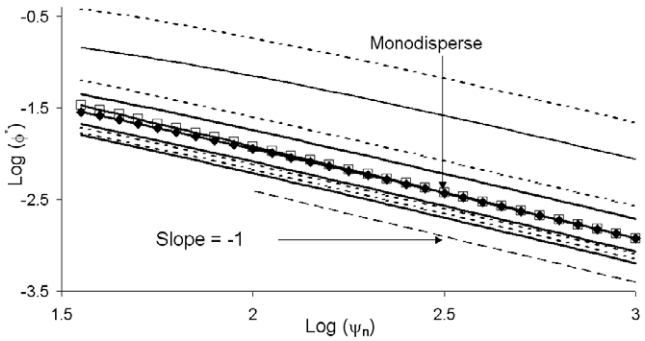

Figure 2. The rod volume fractions at the percolation thresholds $\phi^*_{\rm min}$ and $\phi^*_{\rm max}$ are shown as functions of the number-averaged aspect ratio ψ_n for fixed values of the polydispersity index $P_{\rm L}$. The filled diamonds represent results for a monodisperse system ($P_{\rm L} = 1$) calculated within the present model from equation (4). The open squares represent results for a monodisperse system as calculated from equation (8) of [7], and closely describe the computer simulation results reported in that account for aspect ratios ψ exceeding 20 (see figure 4 of [7]). The curves located above (below) that for the monodisperse system represent results for $\phi^*_{\rm max}(\phi^*_{\rm min})$. The solid and broken lines correspond to results from Type I and Type II models for the rod shape distribution functions, respectively. For the solid as well as the broken lines, $P_{\rm L}$ equals 1.05 and 1.25 for both $\phi^*_{\rm min}$ and $\phi^*_{\rm max}$, in the order of increasing distance from the curve representing the monodisperse system.

the percolation threshold $\phi^*_{\rm min}(\phi^*_{\rm max})$, although the dependence upon ψ_n is largely unaffected. Over the range of volume fractions between $\phi^*_{\rm min}$ and $\phi^*_{\rm max}$, the percolation probability transitions in a continuous manner from being zero (for $\phi < \phi^*_{\rm min}$) to non-zero (for $\phi > \phi^*_{\rm max}$) for all the nanoparticles in the system. The width of the percolation transition, i.e. the separation between $\phi^*_{\rm min}$ and $\phi^*_{\rm max}$, increases dramatically with $P_{\rm L}$ for both polydispersity models considered in the present investigation. This widening is significantly more pronounced for the Type II than for the Type I polydispersity model, and in both cases $\phi^*_{\rm max}$ is predicted to be more sensitive to $P_{\rm L}$ than is $\phi^*_{\rm min}$.

The broadening of the percolation transition seen in figure 2 may provide a partial explanation for the smooth and continuous variation of the modulus as a function of the filler volume fraction which has been observed in cellulose whisker reinforced nanocomposites [1, 2, 19]. For example, the study in [19] attributes an average aspect ratio (ψ_n) of approximately 135 to the dispersed nanoparticles. Equation (4) suggests that the percolation threshold for perfectly monodisperse rods with this value of ψ_n should be approximately $\phi^*_{\rm monodisperse} \approx 8.5 \times 10^{-3}$, i.e. about 0.85% by volume. However, if we instead assume a length polydispersity index of $P_{\rm L} = 1.15$, which is comparable to those reported for nanoparticles derived from cotton linters and commercially available microcrystalline cellulose in [20], the percolation transition (at fixed $\psi_n = 135$) broadens to encompass the volume fraction ranges: $0.513\% < \phi < 2.47\%$ for the Type I, and $0.521\% < \phi < 4.92\%$ for the Type II polydispersity models, respectively. These estimates for $\phi^*_{\rm min}$ and $\phi^*_{\rm max}$ clearly depend strongly upon the specific choice for the distribution function $f(R, L)$, and both employ the assumption of a uniform distribution of rod dimensions (equation (7)). Nevertheless, it is noteworthy that figure 5 of [19] reveals a smooth and continuous increase in the composite shear modulus for volume fractions of up to approximately 6%, in marked contrast to the prediction from a percolation model which does not explicitly address polydispersity effects. Note also that these calculations, as well as those presented in figures 1 and 2, employ the approximation of a uniform distribution function as specified in equation (7). The adoption of a size distribution function characterized by a long, slowly decaying tail (e.g. the Schulz distribution) may be expected to further widen the range of volume fractions which separate $\phi^*_{\rm min}$ from $\phi^*_{\rm max}$.

Polydispersity effects are also likely to play a role in determining critical volume fractions in nanocomposites containing electrically conducting filler particles. As another preliminary application of our present approach, we consider the polyurethane-based composites described in [27], which incorporated cellulose fibres coated with metallic copper. The average radii (assuming the entire fibre surface had been successfully coated) and lengths of the fibres were approximately 23.5 μm and 278 μm, respectively. Based on the histogram of fibre lengths provided in figure 2 of [27], we estimate the largest and smallest fibre lengths $L_{\rm max}$ and $L_{\rm min}$ to have been approximately 700 μm and 50 μm, respectively (a similar histogram was not provided for the fibre diameters). Based on these data, our Type I model for polydispersity (equation (5)) with $\psi_n = 278/23.5 = 11.83$, $L_{\rm max} = 700$ μm, and $R_0 = 23.5$ μm, suggests that $\phi^*_{\rm min} \approx 0.0294$. A comparable calculation within the Type II polydispersity model, employing (i) the parameters $\psi = \psi_n = 11.83$ and $R_{\rm max}/R_{\rm min} = L_{\rm max}/L_{\rm min} = 700/50 = 14$, and (ii) the assumption of a uniform distribution function over fibre radii (equation (7)), yields by way of equation (6) the estimate that $\phi^*_{\rm min} \approx 0.0379$. Equation (4) suggests that a monodisperse population of rods with an aspect ratio of 11.83 would have a percolation threshold of approximately $\phi^*_{\rm monodisperse} \approx 0.0658$. Interestingly, the composites investigated in [27] showed a measurable (although small, of order $\approx 10^{(0)}$ Ω^{-1} m^{-1}) electrical conductance, as well as resonances in the dielectric permittivity, for volume fractions greater than 0.04 (4%). The resonances observed for volume fractions above 4% were attributed to the formation of inter-fibre contacts [27]. It is possible (as suggested in [27, 28]) that the low conductances measured in this regime could have arisen from either (i) incomplete coating of the fibre surfaces, and/or (ii) from weak electrical contacts between the fibres. Given that the instrumental detection threshold for conductance in [27] was estimated as being $\approx 10^{-9}$ Ω^{-1} m^{-1}, the conductivities measured for fibre volume fractions above 4%, although small, nevertheless represent an increase in this quantity by approximately nine orders of magnitude. These observations therefore may not be entirely inconsistent with incipient geometric percolation. It should, however, be emphasized that the close agreement between the values of $\phi^*_{\rm min}$ as calculated within our model and the critical volume fraction above which dielectric resonances and measurable conductivities were observed in [27] is almost

certainly fortuitous, especially in view of the highly non-uniform distribution of fibre lengths reported in that work.

Accounting for the effect of polydispersity upon percolation thresholds will be important in the microscopic modelling of fibre-reinforced composites [29] for such efforts to proceed beyond the invocation of a single, effective aspect ratio [1, 16–18]. Incorporating information regarding the particle size and shape distribution will be especially relevant for nanoparticles derived from lignocellulosic sources, given that the aspect ratios, dimensions, and polydispersities of such filler species depend upon both the method of preparation [30, 31] and their ultimate biological origins [20, 21]. The methodology described in the present account provides a step towards the development of such a theoretical framework, and may also be of value in investigating the formation of conducting pathways in nanocomposites containing SWNTs [23], or metallized cellulose particles [27], or lipid tubules [28].

Acknowledgment

The author expresses his gratitude to Ms Darya A Prokhorova and to Professor William T Winter, both of the Department of Chemistry, SUNY-ESF, for insightful and stimulating suggestions and discussions. The author also thanks Ms DeAnn Barnhart of the same Department for a painstaking and careful proofreading of the manuscript.

References

[1] Samir M A S A, Alloin F and Dufresne A 2005 *Biomacromolecules* **6** 612–26
[2] Favier V, Chanzy H and Cavaille J Y 1995 *Macromolecules* **28** 6365–7
[3] Paillet M and Dufresne A 2001 *Macromolecules* **34** 6527–30
[4] Chatterjee T, Yurekli K, Hadjiev V G and Krishnamoorti R 2005 *Adv. Funct. Mater.* **15** 1832–8
[5] Nobile M R, Simon G P, Valentino O and Morcom M 2007 *Macromol. Symp.* **247** 78–87
[6] Biercuk M J, Llaguno M C, Radosavljevic M, Hyun J K, Johnson A T and Fischer J E 2002 *Appl. Phys. Lett.* **80** 2767–9
[7] Foygel M, Morris R D, Anez D, French S and Sobolev V L 2005 *Phys. Rev.* B **71** 104201
[8] Stauffer D and Aharony A 1991 *Introduction to Percolation Theory* (Philadelphia, PA: Taylor and Francis)
[9] Philipse A P 1996 *Langmuir* **12** 1127–33
[10] Williams S R and Philipse A P 2003 *Phys. Rev.* E **67** 051301
[11] Berhan L and Sastry A M 2007 *Phys. Rev.* E **75** 041120
[12] Balberg I, Binenbaum N and Wagner N 1984 *Phys. Rev. Lett.* **52** 1465–8
[13] Schilling T, Jungblut S and Miller M A 2007 *Phys. Rev. Lett.* **98** 108303
[14] Wang X and Chatterjee A P 2003 *J. Chem. Phys.* **118** 10787–93
[15] Ogata R, Odagaki T and Okazaki K 2005 *J. Phys.: Condens. Matter* **17** 4531–8
[16] Lima M D, Andrade M J, Skakalova V, Bergmann C P and Roth S 2007 *J. Mater. Chem.* **17** 4846–53
[17] Favier V, Dendievel R, Canova G, Cavaille J Y and Gilormini P 1997 *Acta Mater.* **45** 1557–65
[18] Chazeau L, Cavaille J Y, Canova G, Dendievel R and Boutherin B 1999 *J. Appl. Polym. Sci.* **71** 1797–808
[19] Favier V, Canova G R, Shrivastava S C and Cavaille J Y 1997 *Polym. Eng. Sci.* **37** 1732–9
[20] Elazzouzi-Hafraoui S, Nishiyama Y, Putaux J–L, Heux L, Dubreuil F and Rochas C 2008 *Biomacromolecules* **9** 57–65
[21] Beck-Candanedo S, Roman M and Gray D G 2005 *Biomacromolecules* **6** 1048–54
[22] Lu C and Liu J 2006 *J. Phys. Chem.* B **110** 20254–7
[23] Ounaies Z, Park C, Wise K E, Siochi E J and Harrison J S 2003 *Compos. Sci. Technol.* **63** 1637–46
[24] Li J, Cheng Ma P, Sze Chow W, Kai To C, Zhong Tang B and Kim J-K 2007 *Adv. Funct. Mater.* **17** 3207–15
[25] Lu H, Shen H, Song Z, Shing k S, Tao W and Nutt S 2005 *Macromol. Rapid Commun.* **26** 1445–50
[26] Kihara T 1953 *Rev. Mod. Phys.* **25** 831–43
[27] Zabetakis D, Dinderman M and Schoen P 2005 *Adv. Mater.* **17** 734–8
[28] Browning S L, Lodge J, Price R R, Schelleng J, Schoen P E and Zabetakis D 1998 *J. Appl. Phys.* **84** 6109–13
[29] Chatterjee A P and Prokhorova D A 2007 *J. Appl. Phys.* **101** 104301
[30] Wang N, Ding E and Cheng R 2007 *Polymer* **48** 3486–93
[31] Zhang J, Elder T J, Pu Y and Ragauskas A J 2007 *Carbohydr. Polym.* **69** 607–11